

# Revealing the role played by $\alpha$ - and $\beta$ -relaxation in hydrostatically compressed metallic glasses

Jie Shen<sup>1,2†\*</sup>, Antoine Cornet<sup>1,2†</sup>, Alberto Ronca<sup>1,2</sup>, Eloi Pineda<sup>3</sup>, Fan Yang<sup>4</sup>, Jean-Luc Garden<sup>1</sup>, Gael Moiroux<sup>1</sup>, Gavin Vaughan<sup>2</sup>, Marco di Michiel<sup>2</sup>, Gaston Garbarino<sup>2</sup>, Fabian Westermeier<sup>5</sup>, Celine Goujon<sup>1</sup>, Murielle Legendre<sup>1</sup>, Jiliang Liu<sup>2</sup>, Daniele Cangialosi<sup>6,7</sup> and Beatrice Ruta<sup>1,2\*</sup>

<sup>1</sup> Institut Néel, Université Grenoble Alpes and Centre National de la Recherche Scientifique, 25 rue des Martyrs - BP 166, 38042, Grenoble cedex 9, France

<sup>2</sup> European Synchrotron Radiation Facility, 71 avenue des Martyrs, CS 40220, Grenoble 38043, France

<sup>3</sup> Department of physics, Institute of Energy Technologies, Center for Research in Multiscale Science and Engineering, Universitat Politècnica de Catalunya-BarcelonaTech, 08019 Barcelona, Spain

<sup>4</sup> Institut für Materialphysik im Weltraum, Deutsches Zentrum für Luft- und Raumfahrt (DLR), 51170 Köln, Germany

<sup>5</sup> Deutsches Elektronen-Synchrotron DESY, Notkestraße 85, D-22607 Hamburg, Germany

<sup>6</sup> Donostia International Physics Center, Paseo Manuel de Lardizabal 4, 20018 San Sebastián, Spain

<sup>7</sup> Centro de Física de Materiales (CSIC–UPV/EHU), Paseo Manuel de Lardizabal 5, 20018 San Sebastián, Spain

† These authors equally contributed

\*corresponding authors

[jie.shen@neel.cnrs.fr](mailto:jie.shen@neel.cnrs.fr)

[beatrice.ruta@neel.cnrs.fr](mailto:beatrice.ruta@neel.cnrs.fr)

## **Abstract:**

Any property of metallic glasses is controlled by the microscopic ongoing relaxation processes. While the response of these processes to temperature is well documented, little is known on their pressure dependence, owing to non-trivial experimental challenges. By combining fast differential scanning calorimetry, X-ray diffraction and high-pressure technologies, we identify the origin of a recently discovered pressure-induced rejuvenation in metallic glasses from the different pressure response of the  $\alpha$ - and  $\beta$ -relaxation in a series of hydrostatically compressed Vit4 glasses. While the localized  $\beta$ -relaxation promotes rejuvenation and is associated to a constant looser atomic packing independent of the applied pressure, the collective  $\alpha$ -relaxation triggers density driven ordering processes promoting the stability. The latter parameter however cannot be solely described by the degree of equilibration reached during the compression, which instead determines the crossover between the two regimes allowing to rescale the corresponding activation energies of the two processes on a master curve.

## **Introduction:**

Understanding the relaxation spectrum of metallic glass (MG)-formers is a great challenge in condensed matter physics and materials science with important technological implications, as relaxation modes play a prominent role in the aging and performance of glasses [1-5]. The structural relaxation process, also called  $\alpha$ -relaxation, is responsible for the viscous flow in the liquid phase and it involves large cooperative rearrangements. Its temperature evolution in supercooled liquids determines the kinetic fragility of the material, a quantity that correlates with a large variety of material properties and allows classifying glass-formers in fragile and strong systems [6]. The secondary  $\beta$ -relaxation is instead related to the thermal activation of localized atomic mobility and persists also at temperatures much lower than the glass transition temperature,  $T_g$  [7-10]. Additional secondary processes, such as  $\gamma$ - and  $\beta'$ -relaxations, have been also identified in several glasses, and can be attributed to string-like motions far below  $T_g$  [11-15]. While

countless studies have highlighted the strong dependence of many macroscopic properties on the relaxation dynamics [4,15-18], almost no signature of the different processes has been detected on the microscopic structure [19,20].

Hydrostatic pressure can significantly modify the relaxation spectrum of glass-formers. In molecular, ionic, and polymeric systems, dielectric experiments indicate that  $\alpha$ -relaxation considerably slows down under high pressure, shifting  $T_g$  to higher values [21-23]. In contrast, secondary  $\beta$ -relaxation processes are less sensitive to pressure and exhibit a different response to isothermal compressions and isobaric thermal treatments. As a consequence, high pressure leads to a larger difference in time scales between  $\alpha$ - and  $\beta$ -relaxation, and the impossibility to rescale the whole dynamics in a single master curve [24,25].

In the case of MGs, still little is known on the pressure response of the relaxation processes due to the difficulty to apply *in-situ* hydrostatic compression. Recently, we developed an *in-situ* X-ray photon correlation spectroscopy (XPCS) setup that allows the measurement of the dynamics of supercooled metallic liquids under high-temperature and high-pressure conditions [26]. Our work shows an increasingly sluggish  $\alpha$ -relaxation under *in-situ* high pressure, similarly to that reported in other families of glass-formers [21-23], and in agreement with molecular dynamic simulations [27]. However, due to technical limitations in the accessible time scales, no information on the pressure dependence of the  $\beta$ -relaxation process can yet be obtained.

To circumvent the experimental challenges of performing *in-situ* high pressure measurements, many studies have focused on the pressure response of pre-densified MGs. In these cases, the material is first compressed at a given pressure and temperature, and subsequently studied after recovering the resulting glass at ambient conditions. The recovered materials contain therefore information on the glass ability to retain permanent densification after decompression from pressures exceeding their plasticity limit. For example, SiO<sub>2</sub> glass exhibits a density increase of over 20% at ambient conditions when previously subjected to pressures greater than 21 GPa [28]. In the case of MGs, a 1-2% increase in density has been reported in samples previously compressed at room temperature at 5.5-20 GPa [28-30], while recent *in-situ* high pressure X-ray diffraction

(XRD) experiments have indicated the absence of important permanent structural changes in Zr-based MG even densified up to 30 GPa at room temperature [31].

In MGs, the effects of high-pressure compression depend also on the applied temperature. Researchers have shown that isobaric quenching from the supercooled liquid under high pressure can enhance thermodynamic stability [32,33]. However, most glasses compressed at temperatures below their respective  $T_g(P)$  are found to be in a higher energy state than the pristine glass [29,30,34-37]. This pressure-induced rejuvenation is accompanied by an unexpected acceleration of the collective atomic motion under high pressure [38], which persists even after the pressure is released [39]. Understanding the pressure response of the different relaxation processes active in the probed temperature range and their relation to the microscopic atomic motion [15,40-42] and structural rearrangements [19,20] is thus essential for a proper comprehension of the response of MGs to pressure treatments.

For this purpose, we conducted a systematic study of the thermal response and structure of a series of  $Zr_{46.25}Ti_{8.25}Cu_{7.5}Ni_{10}Be_{27.5}$  (Vit4) MGs previously compressed at various pressures in the 1-7 GPa range, and for temperatures covering cold compression at ambient temperature, hot compression in the glassy state, and liquid compression in the supercooled liquid phase. We find that pressure shifts the  $\beta$ -to- $\alpha$  relaxation transition to higher temperatures, which scales with the pressure dependence of the glass transition temperature  $T_g(P)$ . Furthermore, the nature of the relaxation process active during the compression protocol controls the thermal response and structure of the resulting glasses. The  $\beta$ -relaxation promotes rejuvenation and is associated with a looser atomic packing that is independent on the applied pressure and density, while the  $\alpha$ -relaxation involves larger-scale structural rearrangements and achieves glass stabilization through a pressure-dependent densification process. Our study highlights the critical role of relaxation processes in the response to hydrostatic pressure treatment of a prototypical strong metallic glass, providing clear thermo-mechanical processing guidelines for designing glasses with the same composition but different properties.

## Results

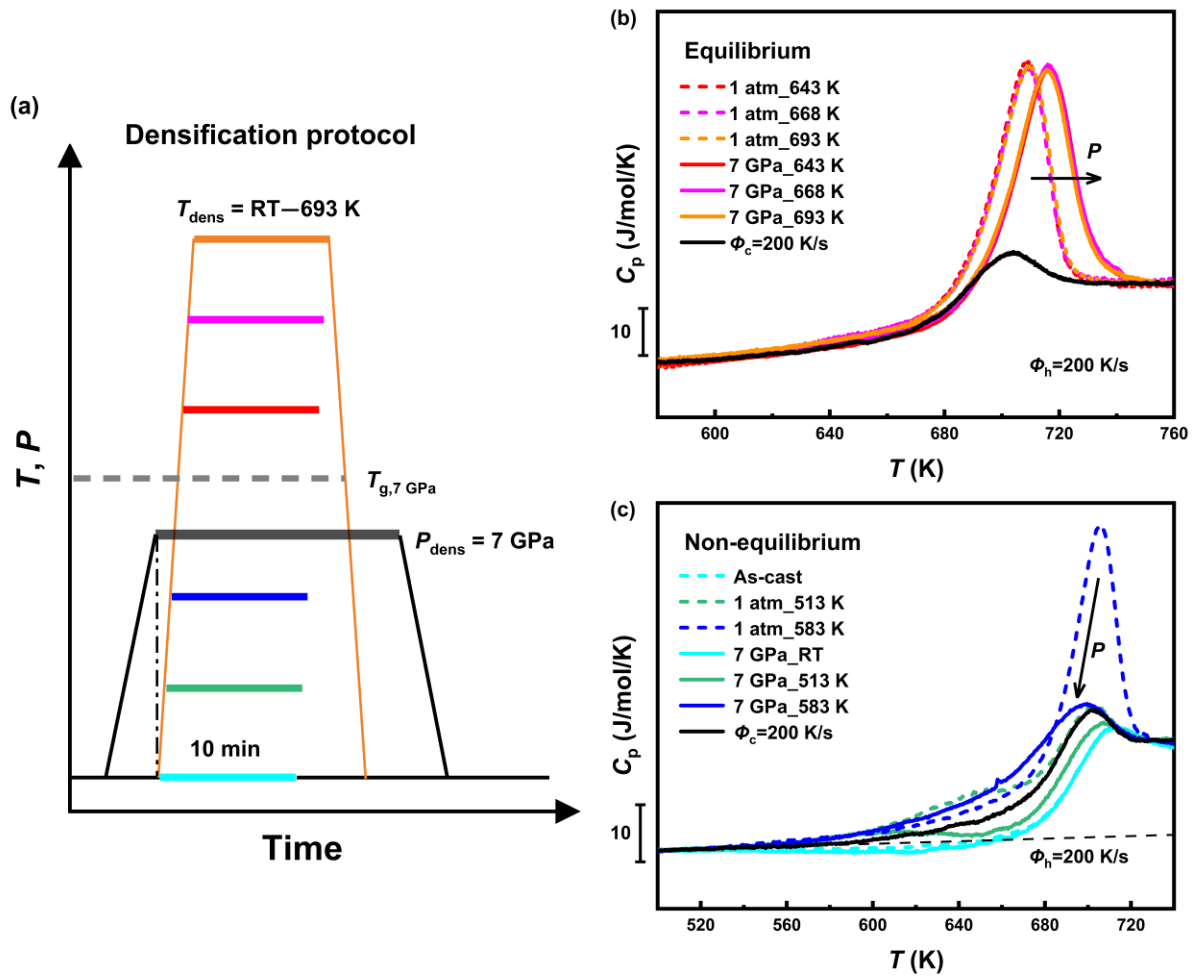


**Figure 1. Thermodynamic state of ex-situ compressed glasses.** (a) Sketch of the densification protocol. First pressure is increased at the  $P_{\text{dens}} = 7 \text{ GPa}$ , and then for each sample the temperature is raised to a fixed value  $T_{\text{dens}}$ , ranging from 298 K to 693 K for 10 min. When  $T_{\text{dens}} > T_g(P)$ , the sample under compression is in thermodynamic equilibrium; when  $T_{\text{dens}} < T_g(P)$ , it is in a thermodynamic non-equilibrium state. The temperature is then cooled back to the ambient value with a rate of 20 K/min prior to the release of the pressure. The resulting glasses are then recovered at ambient condition for calorimetry measurements. (b) and (c) Selection of calorimetry heating curves measured with FDSC at 200 K/s for samples previously compressed at 7 GPa and  $T_{\text{dens}} \geq 643 \text{ K}$  (b) and at  $T_{\text{dens}} \leq 583 \text{ K}$  (c). Reference data of samples pre-annealed at annealing temperatures  $T_a = T_{\text{dens}}$  and ambient pressure (dashed lines) are reported as well for comparison, together with data acquired in

a glass cooled from the supercooled liquid state with a rate  $\Phi_c = 200$  K/s equal to the heating rate used immediately after for the measurements (black line).

**Pressure dependence of the relaxation spectrum.** In compression experiments, the properties of the material are influenced by both the densification pressure,  $P_{\text{dens}}$ , and the densification temperature,  $T_{\text{dens}}$ . To explore the effect of  $T_{\text{dens}}$ , we first employed an isobaric densification protocol and prepared different samples by maintaining a constant  $P_{\text{dens}}$  of 7 GPa and varying  $T_{\text{dens}}$  from 298 to 693 K (from the deep glass state to the fully-equilibrated supercooled liquid phase) (**Fig. 1a**). The resulting glasses were then studied by single shot flash differential scanning calorimetry (FDSC) [34] and synchrotron x-ray diffraction. **Fig. 1b** and **1c** display FDSC curves of the compressed glasses. Reference samples subjected to the same temperature protocols but at 1 atm are reported as well. In a single shot FDSC experiment, the sample is measured without the usual melting on chip to preserve the properties induced by the densification process. The validity of this approach as well as the reproducibility of the data is discussed in the methods (see also **Fig. S1**). The scans were performed using a heating rate,  $\Phi_h$ , of 200 K/s, much faster than the cooling rate of 20 K/min employed during the densification protocols. This approach allows to preserve the effect of the densification up to the glass transition and generates an amplified overshoot peak in the curves [43], enabling a better comparison of the thermodynamic state among the different samples. As a reference, we also show the heating scan of a sample cooled from the supercooled liquid at 200 K/s, and immediately heated at the same rate. This scan markedly differs from those of samples mildly annealed at atmospheric pressure due to the much faster cooling rate.

In agreement with our previous work [34], we find that it is possible to get both thermal relaxation and rejuvenation by varying  $T_{\text{dens}}$ . For samples compressed at 7 GPa from  $T_{\text{dens}} \geq 643$  K,  $T_{\text{g,onset}}$  shifts by 6 K to larger values (**Fig. 1b**). This shift corresponds to an increase in the glass transition temperature  $\left(\frac{\partial T_{\text{g,onset}}}{\partial P}\right)_{\text{ex-situ}} = 0.86$  K/GPa in the plastically deformed glasses and strongly recalls the increased stability observed in Pt-based MGs quenched under pressure from the supercooled liquid [34], supporting that Vit4 is in equilibrium during the densification protocol.

This consideration is supported also by the independence of the calorimetric response from the choice of  $T_{\text{dens}}(\geq 643)$  K. As shown in **Fig 1b**, all curves overlap on top of each other as it occurs also for the reference glasses which are all quenched from the corresponding supercooled liquid at 1 atm ( $T_g(1 \text{ atm})=596$  K, [44]). These observations imply  $T_g(7 \text{ GPa})$  is  $\leq 643$  K, in agreement also with previous ex-situ studies which suggest a 3.6 K/GPa increase of  $T_g$  under pressure [32], which would correspond to  $T_g(7 \text{ GPa})\sim 621$  K, i.e. much lower than our densification temperatures.

Rejuvenation is instead observed for glasses compressed at 7 GPa and  $T_{\text{dens}} \leq 583$  K, i.e. below  $T_g(1 \text{ atm})$ . This result contrasts the increased endothermic contribution of the references pre-annealed glasses at 1 atm. Furthermore, the thermodynamic state of the compressed material varies with  $T_{\text{dens}}$ , reflecting the response of different metastable glassy states formed during high-pressure annealing in the glassy state (**Fig. 1c**). At this pressure, lowering the annealing temperature shifts the main endothermic peak to a sub- $T_g$  endothermic contribution, corresponding to the curve change from  $T_a=583$  K to 513 K in **Fig. 1c**. This evolution is common in the aging of MGs and is attributed to a shift from  $\alpha$ -relaxation-dominated dynamics at high temperatures to more localized particle motion driven by the  $\beta$ -relaxation in deep glassy states [45,46]. This behavior is universal as it is observed in other kinds of glasses, such as inorganic [47] and polymeric glasses [48]. In the compressed glasses at  $T_{\text{dens}}=583$  K and 513 K, the sub- $T_g$  endothermic peak appears with significantly reduced intensity. In the extreme case of 298 K (well below  $T_g$ ), the heat flow curve shows a slightly broader exothermic peak compared to the sample obtained in the same conditions but at ambient pressure.

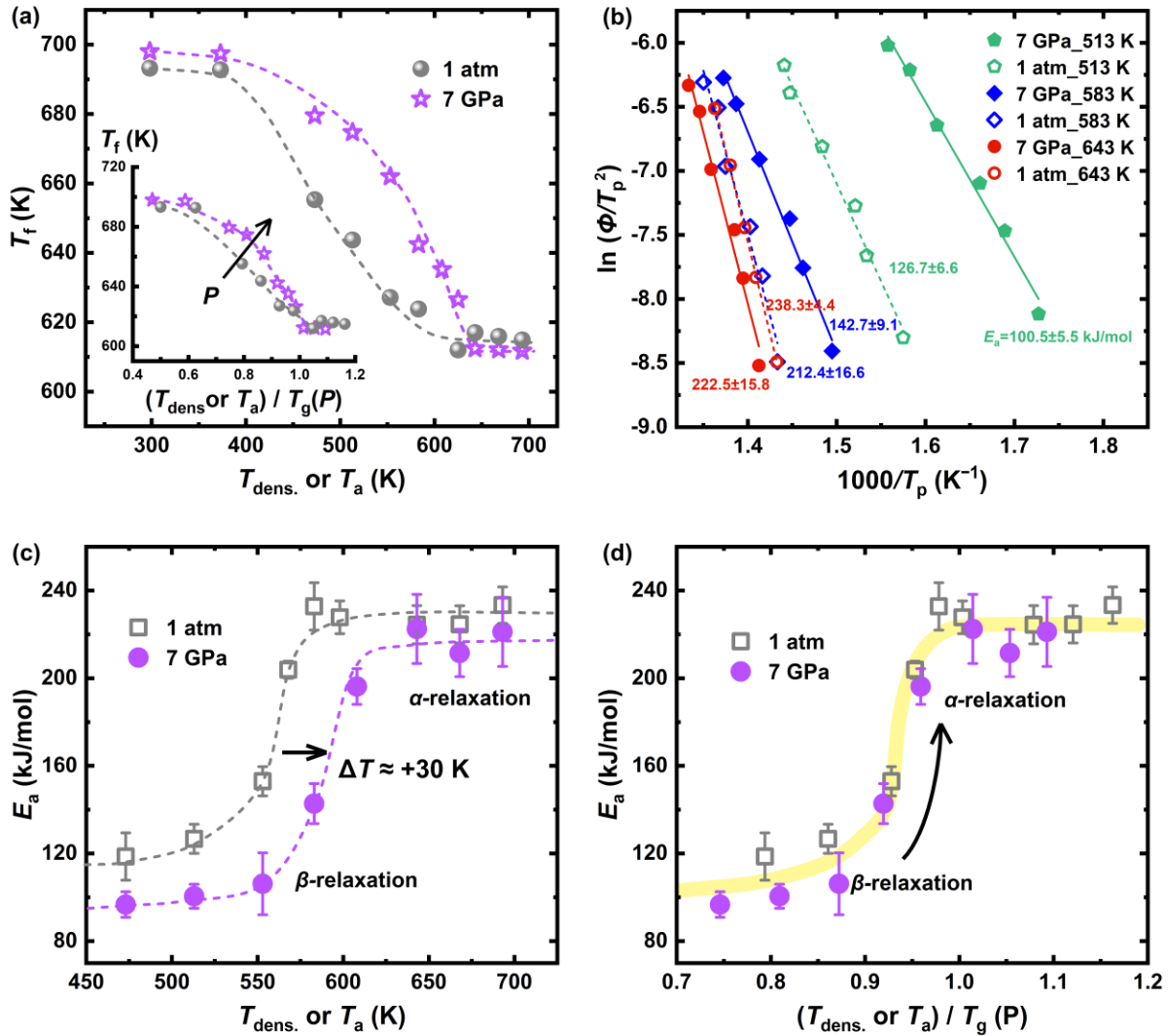


**Figure 2. Pressure dependence of the aging kinetics and relaxation spectrum.** (a) Fictive temperature,  $T_f$  of different annealed and compressed glasses as a function of  $T_{\text{dens.}}$  or  $T_a$ . Inset is the  $T_f$  of different annealed and compressed glasses as a function of  $T_{\text{dens.}}$  and  $T_a$  normalized by the corresponding  $T_g(P)$ , where the arrow indicates the shift in  $T_f$  under pressure. (b) Kissinger plot illustrating the characteristic temperature,  $T_p$ , of the endothermic peak (see Fig. S2 for definition) in the FDSC curves as a function of the heating rate  $\Phi_h$  for different annealed and compressed glasses. (c) Activation energy,  $E_a$  of different annealed and compressed glasses. The data are reported as a function of  $T_{\text{dens.}}$  or  $T_a$ . Only data displaying a clear endothermic peak have been used for the analysis of the activation energies. (d)  $E_a$  of different annealed and compressed glasses as a function of  $T_{\text{dens.}}$  and  $T_a$  normalized by the corresponding  $T_g(P)$ . The arrow indicates the transition from  $\beta$ -relaxation to  $\alpha$ -



relaxation.

By using Moynihan's area-matching method in the calorimetric scans [49], we can confirm the previous observations from the evaluation of the fictive temperature,  $T_f$ . Since the FDSC measurements were conducted at 1 atm, it is worth noting that  $T_f$  in this work is used as a metric for the thermodynamic state (see **Fig. S3** for further details) and does not reflect the real temperature at which vitrification occurs under high pressure. **Fig. 2a** reports the  $T_f$  obtained in glasses densified at 7 GPa and different temperatures between 298 K and 693 K. Reference values for glasses annealed at the same temperatures and 1 atm are reported as well. In both sets of glasses,  $T_f$  evolves with the annealing or densification temperature from a maximum value at low temperatures, signature of a frozen glass configuration, to an increasingly lower value at larger  $T_a$  and  $T_{\text{dens}}$ , a consequence of thermally-activated microscopic structural rearrangements occurring in the material [50].  $T_{\text{dens}}$  modifies the value of  $T_f$  in a non-monotonic way. For  $T_{\text{dens}}$  lower than 400 K, the glasses compressed at 7 GPa are only slightly rejuvenated with a constant increase in  $T_f$  independently on the applied temperature during the densification. Differently, glasses densified at 7 GPa between 400 K and 630 K have systematically larger  $T_f$  by  $\sim 30$  K (compared to samples annealed at the same temperature under 1 atm), signalling a more enhanced rejuvenation in this temperature range. In contrast, for  $T_{\text{dens}} \geq 643$  K  $T_f$  decreases to a  $T$ -independent lower value (by 3-4 K) with respect to the 1 atm data. The glass obtained from compressed liquid shows a higher  $T_{\text{g,onset}}$  and a lower  $T_f$ , reflecting a more relaxed state, which aligns with the behavior reported in Pt-based MG [34]. This relaxed state is further evidenced by the increased area of the endothermic peak (**Fig. S4**). Furthermore, the broadening of the endothermic peak in the compressed glass (**Fig. 1b** and **Fig. S4**) indicates a modification in the process of glass transition, possibly associated with dynamical and structural transformation of the system under high pressure [27].

To get the activation energies associated with the different relaxation processes responsible for the observed kinetic stability, **Fig. 2b** shows Kissinger plots of glasses annealed and compressed under different  $T_a$  or  $T_{\text{dens}}$  and then measured with FDSC at different heating rates

[45,51]. We outline here that for the densified glasses, each point corresponds to a new sample. The corresponding activation energies obtained by fitting the data are shown in **Fig. 2c**. The activation energies distinctly evolve between two extreme values on increasing the annealing temperature,  $T_a$ , in the reference glasses or  $T_{\text{dens}}$  in the compressed MGs. These values are close to those reported in literature for the  $\beta$ - and  $\alpha$ -relaxation processes, respectively ( $\sim 28 RT_{g,1\text{atm}}$  for the  $\beta$ -process, and  $\sim 42 RT_{g,1\text{atm}}$  for the  $\alpha$ -relaxation [10,52,53]). As shown in **Fig. 2c**, pressure shifts the crossover between the two values by  $\sim 30$  K at 7 GPa. This means that applying hydrostatic pressure at temperatures slightly below  $T_g(1\text{ atm})$  can induce a transition in the dominant relaxation mode, explaining thus the difference between annealing and thermal compression. At 583 K, for instance, the significant decrease in activation energy for samples compressed at 7 GPa suggests that the  $\alpha$ -relaxation is notably suppressed, leaving only the unrestricted localized atoms active, contributing to the  $\beta$ -relaxation observed as the sub- $T_g$  endothermic peak. At the same temperature, however, the dynamics at 1 atm is still governed by the  $\alpha$ -structural relaxation, explaining the improved stability during annealing. For  $T_{\text{dens}} \geq 643$  K, the constant activation energy indicates that  $\alpha$ -relaxation is fully activated also at 7 GPa and both pressures give similar activation energies.

The pressure dependence of the crossover between the  $\alpha$ - and  $\beta$ -dominated relaxation dynamics is responsible for the different stability of the high pressure annealed glasses. Comparing the  $T_f$  and  $E_a$  values, we can divide the  $T_{\text{dens}}$  space into three regions: (I) the cold compression region where temperature effects are almost negligible in this composition. Here, the slightly larger exothermic peak area after compressions indicates a purely mechanical rejuvenation; (II) the temperature-pressure coupling region: here, pressure delays the transition between  $\beta$ - and  $\alpha$ -relaxation leading to a significant rejuvenation in compressed glasses with  $T_f$  much larger than in annealed systems whose response is instead more controlled by the  $\alpha$ -relaxation; (III) the equilibrium region, accompanied by a complete activation of the  $\alpha$ -relaxation: here compression leads to a sample stabilization as manifested by a decrease in  $T_f$ . In this region,  $T_f$  and  $E_a$  are constant, indicating that the system has reached a state of thermodynamic equilibrium for  $T \gtrsim 625$  K. This means that during the densification process the transition between the glass and the

supercooled liquid occurs between 625 K and 643 K (where equilibrium is achieved). Taking the midpoint of 634 K, we designate it as the  $T_g$  under *in-situ* compression at 7 GPa, and thus to  $\left(\frac{\partial T_g}{\partial P}\right)_{\text{in-situ}} = 5.4$  K/GPa, a factor of two smaller than the value measured *in-situ* at high pressure in Pt<sub>42.5</sub>Cu<sub>27</sub>Ni<sub>9.5</sub>P<sub>21</sub> [34], reflecting the different sensitivities to pressure of the strong Vit4 and the fragile Pt-based metallic glasses.

The correct evaluation of  $T_g(P)$  is also confirmed by the possibility to rescale all activation energy data in a unique master curve when the temperature is rescaled by the corresponding glass transition temperature at the applied pressure (**Fig. 2d**). This means that the  $\beta$ - to  $\alpha$ -relaxation transition range occurs always at the same degree of equilibration, independently of the applied pressure, which corresponds to 0.85–0.96  $T_g(P)$ .

Interestingly, while the relaxation spectrum can be scaled into a single curve, this is not the case for  $T_f$ . The inset in **Fig. 2a** and the comparison of FDSC curves in **Fig. S5** show that, even when normalized by  $T_g(P)$ , there is still a large difference in the  $T_f$  values at the two pressures, with a nonmonotonic trend exhibiting a maximum difference at about 0.85  $T_g(P)$ , followed by a gradually decrease at increasingly  $T_{\text{dens}}$  or  $T_a$ , until both values almost overlap in the supercooled liquid (see also **Fig. 3e** which shows the ratio  $T_f(7 \text{ GPa})/T_f(1 \text{ atm})$ ). The largest difference in fictive temperature corresponds to the beginning of the  $\beta$ -to- $\alpha$  relaxation transition. This indicates that the increase in  $T_f$  cannot be solely attributed to the reduced aging kinetics caused by the increase in  $T_g$  under high pressure—but to a different response to pressure of the two microscopic processes. As confirmed also by the structural measurements discussed later in the text, the different evolution of  $T_f$  at the two pressures implies that  $\beta$ -relaxation facilitates rejuvenation of the sample under high pressure, whereas  $\alpha$ -relaxation contributes to accelerated aging (evidenced by the steeper slope in the evolution of  $T_f(7 \text{ GPa})/T_f(1 \text{ atm})$  above 0.85  $T_g(P)$  in **Fig. 3e**).

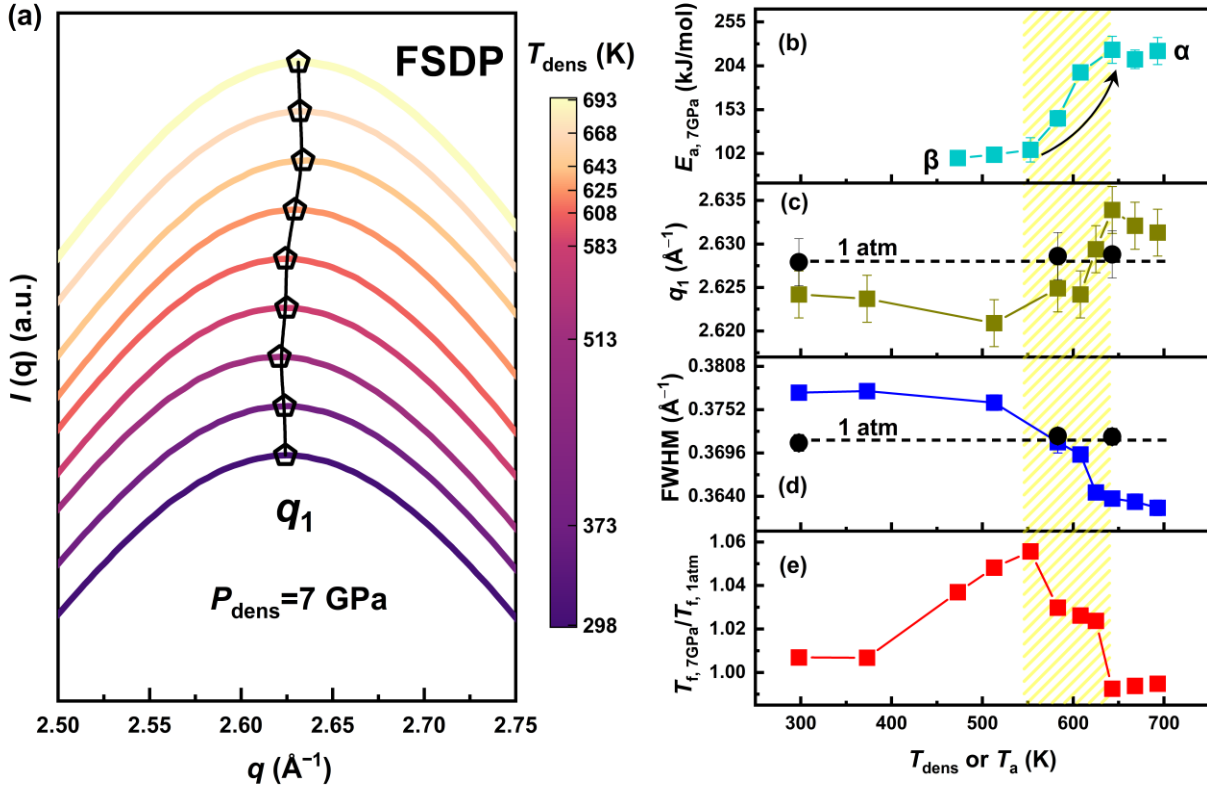


**Figure 3. Structural properties of annealed and compressed glasses.** (a) Intensity profile,  $I(q)$ , measured at ambient temperature with synchrotron XRD in glasses previously compressed at 7 GPa and different  $T_{\text{dens}}$ . The black symbols show the center position,  $q_1$  of the FSDP obtained with a Gaussian fit to the top of the peak (see Fig. S6 and S7, only upper 50% of the peak are fitted). Evolution of calorimetric and structural parameters of glasses densified at 7 GPa and at various  $T_{\text{dens}}$ . Data represent:  $E_a$  (b),  $q_1$  of the FSDP (c), FWHM of the FSDP (d), and the normalized  $T_f$  (e). Reference data for annealed glasses at 1 atm are also included (black circles). The error in  $q_1$  is determined by the maximum deviation (sample thickness) in the sample-to-detector distance for each measurement, while the error in FWHM arises from the fitting uncertainties. The shaded area highlights the temperature transition region from  $\beta$ -relaxation to  $\alpha$ -relaxation determined by the calorimetric measurements.

**Influence of pressure on the structure in compressed glasses.** The different response of  $\alpha$ - and  $\beta$ -relaxation to pressure is reflected also in a contrasting evolution of the structure in the two dynamical ranges. Fig. 3a displays the top part of the first sharp diffraction peaks (FSDP) measured at ambient temperature by means of synchrotron X-ray diffraction in glasses compressed

at 7 GPa and different  $T_{\text{dens}}$ . The center position of the FSDP,  $q_1$  - a quantity often related to the sample density [54] - clearly shows two different regimes. It is almost constant up to  $T_{\text{dens}} \sim 600\text{K}$ , while it shifts to larger  $q$  values at further increasing densification temperatures. As shown in **Fig. 3b** and **3c**, the crossover between these two regimes correlates with the change in the microscopic process active during the compression. A different structural evolution in the two regimes occurs also for the full width half maximum (FWHM) of the FSDP reported in **Fig. 3d**, which describes the degree of homogeneity of the structure at the probed length scale [55]. For a proper interpretation of the data, the figure also includes structural values corresponding to glasses annealed at 1 atm and several selected  $T_a$ .

We first consider the samples subjected to solely temperature annealing. Here, the structure of the glass is almost insensitive to the applied thermal treatment, with only a small increase in  $q_1$  observed at larger  $T_a$ , reflecting a more compact structure, in agreement with previous studies [54,56]. Differently, pressure affects the structure in a non-monotonic way with respect to the pure annealed samples which depends on the densification temperature and thus on the relaxation process active during the compression.

Compared to the reference samples annealed at 1 atm, when the densification temperature ( $T_{\text{dens}}$ ) is far below  $T_g$  (i.e., 298–400 K), the compressed glasses exhibit smaller  $q_1$  and larger FWHM values. This indicates that the plastic deformations induced by the compression lead to structural expansion and increased heterogeneity in the sample. This effect is promoted by the  $\beta$ -relaxation showing a maximum expansion (and thus a minimum in  $q_1$ ) for  $T_{\text{dens}} = 513\text{ K}$ . In the  $\beta$ -to  $\alpha$ -relaxation transition region (e.g.,  $\sim 583\text{ K}$ ), the glass starts to relax during the compression protocol due to the activation of the  $\alpha$ -process and  $q_1$  increases to a value higher than that of the reference glasses. At the same time, the FWHM decreases, meaning that in this  $T_{\text{dens}}$  range, pressure promotes the formation of a more packed and homogenous structure. In the supercooled liquid state,  $q_1$  and FWHM become almost independent of  $T_{\text{dens}}$  within the error bars, which is consistent with the constant thermodynamic stability (**Figs. 1b** and **2a**), indicating that the sample reached the equilibrium state under compression. Interestingly, the rapid variation in  $E_a$  during the

activation of the  $\alpha$ -relaxation is reflected in both structural parameters which show a steeper evolution with  $T_{\text{dens}}$ , in agreement also with the rate of change in fictive temperature (**Fig. 3e**).

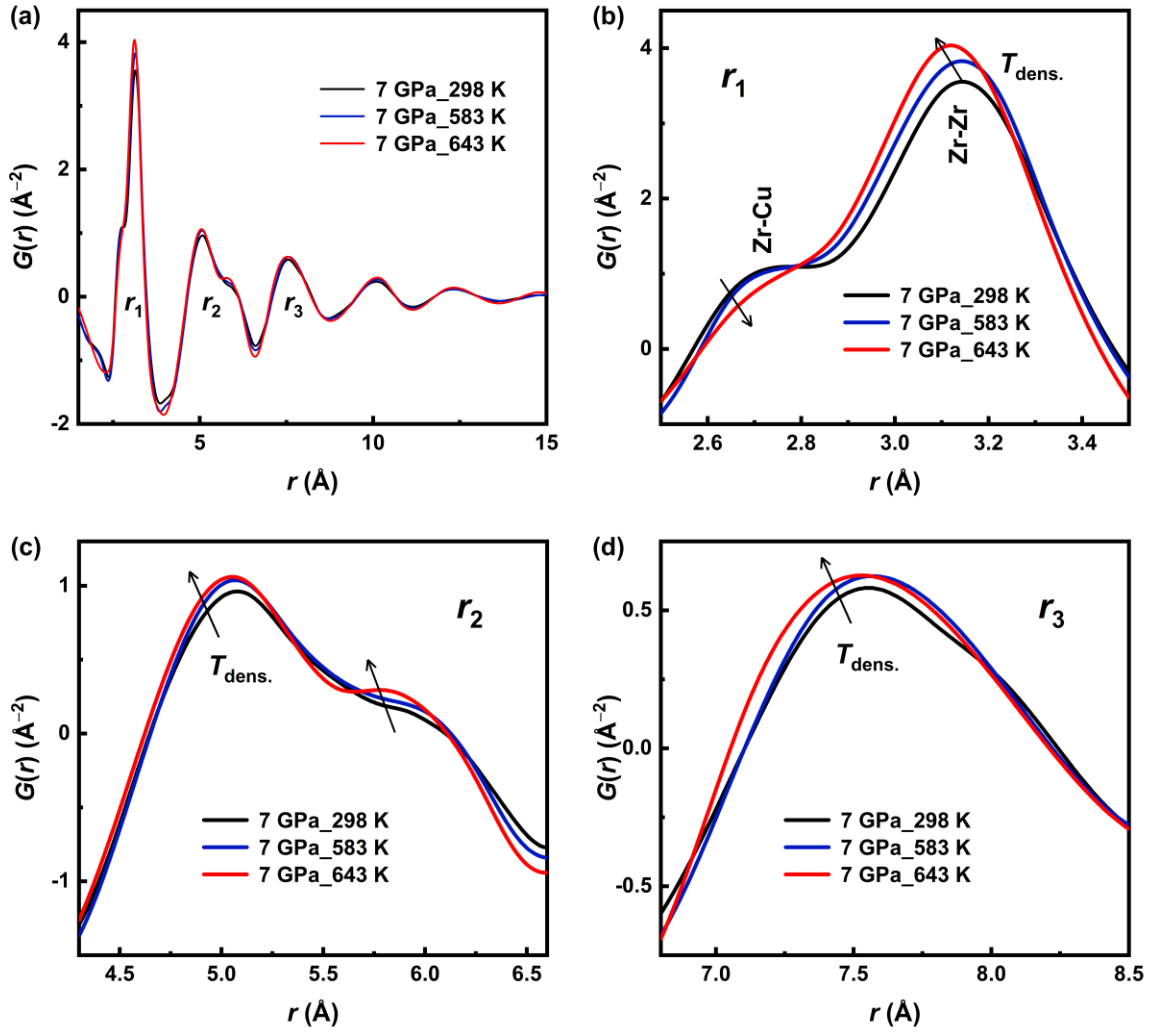


**Figure 4. Real space analysis after densification at different  $T_{\text{dens}}$ .** (a) Pair distribution function,  $G(r)$ , of Vit4 glasses compressed at 7 GPa and  $T_{\text{dens.}}=298$  K (cold compression), 583 K (hot-glass-compression), and 643 K (liquid-compression). (b-d) Close-up views of the 1<sup>st</sup> to 3<sup>rd</sup> atomic coordination peaks of  $G(r)$ , with arrows indicating the direction of changes in each peak as  $T_{\text{dens}}$  increases. The sub-peak and main peak in (b) are primarily corresponding to Zr-Cu and Zr-Zr atomic pairs [57], respectively.

From a structural point of view, we can get further insights on the changes inferred by pressure

during the densification processes by performing pair distribution function analysis of synchrotron XRD data covering a broader  $q$ -range up to  $30 \text{ \AA}^{-1}$ . The obtained pair distribution functions,  $G(r)$ , reveal the detailed atomic structure (particularly on the short-to-medium range scale), from the Fourier transform of the static structure factor (see Methods). **Fig. 4a** shows  $G(r)$  for three samples measured at ambient temperature and 1atm, previously compressed at 7 GPa and for three representative temperatures: i)  $T_{\text{dens}} = 298 \text{ K}$  representing the cold-compression at ambient temperature, ii)  $T_{\text{dens}} = 583 \text{ K}$  which corresponds to the onset of the transition region, and iii)  $T_{\text{dens}} = 643 \text{ K}$  where the system is in the supercooled liquid phase and the  $\alpha$ -relaxation is active. In the two samples densified in the glassy state and affected mainly by  $\beta$ -relaxation (i.e. for  $T_{\text{dens}} = 298$  and  $583 \text{ K}$ ), we observe only changes in the intensity of the peaks of the different coordination shells, signaling a more ordered structure in the glass densified at higher temperatures. The structure is instead clearly different at  $T_{\text{dens}} = 643 \text{ K}$ , i.e. when the compression is triggered by the  $\alpha$ -relaxation, with the significant changes mainly occurring in the first three atomic shells (**Fig. 4b to 4d**).

In the low  $T_{\text{dens}}$  temperature  $\beta$ -relaxation dominated regime, the first coordination shell consists of a sub-peak around  $2.7 \text{ \AA}$  and a main peak around  $3.1 \text{ \AA}$  due to the nearly discrete bonding length distribution of nearest-neighbor atoms. The known interatomic distances indicate that the sub-peak at  $2.7 \text{ \AA}$  can be primarily attributed to Zr-Cu pairs, while the main peak around  $3.1 \text{ \AA}$  corresponds mainly to Zr-Zr pairs [57]. By compression in the supercooled liquid phase, the sub-peak intensity is significantly reduced, while the main peak becomes more intense and shifts to shorter distances, signaling a structural contraction triggered by the  $\alpha$ -relaxation process in agreement with the reciprocal space data of **Fig. 3c**. Based on these changes, it is suggested that the crossover between the  $\beta$ - and  $\alpha$ -relaxation is accompanied by a redistribution of atomic pairs, reflected in a decrease in Cu-Zr bonds and in an increase in Zr-Zr bonds, together with a reduction in their bond distance.

A contraction of the coordination shells for the glass densified at high temperature in the  $\alpha$ -regime is well visible also at larger coordination shells, suggesting a marked densification of the

material during the compression in the liquid phase. Additionally, the clearer oscillations within each shell (increased peak intensity) in the high-pressure  $\alpha$ -relaxation sample, suggest a more ordered atomic structure, consistent with the narrowing of the FSDP (Fig. 3d). Unfortunately, beyond the third atomic shell, the diffraction signal becomes relatively noisy for a proper comparison between the samples; therefore, discussions at larger atomic scales are not involved here.

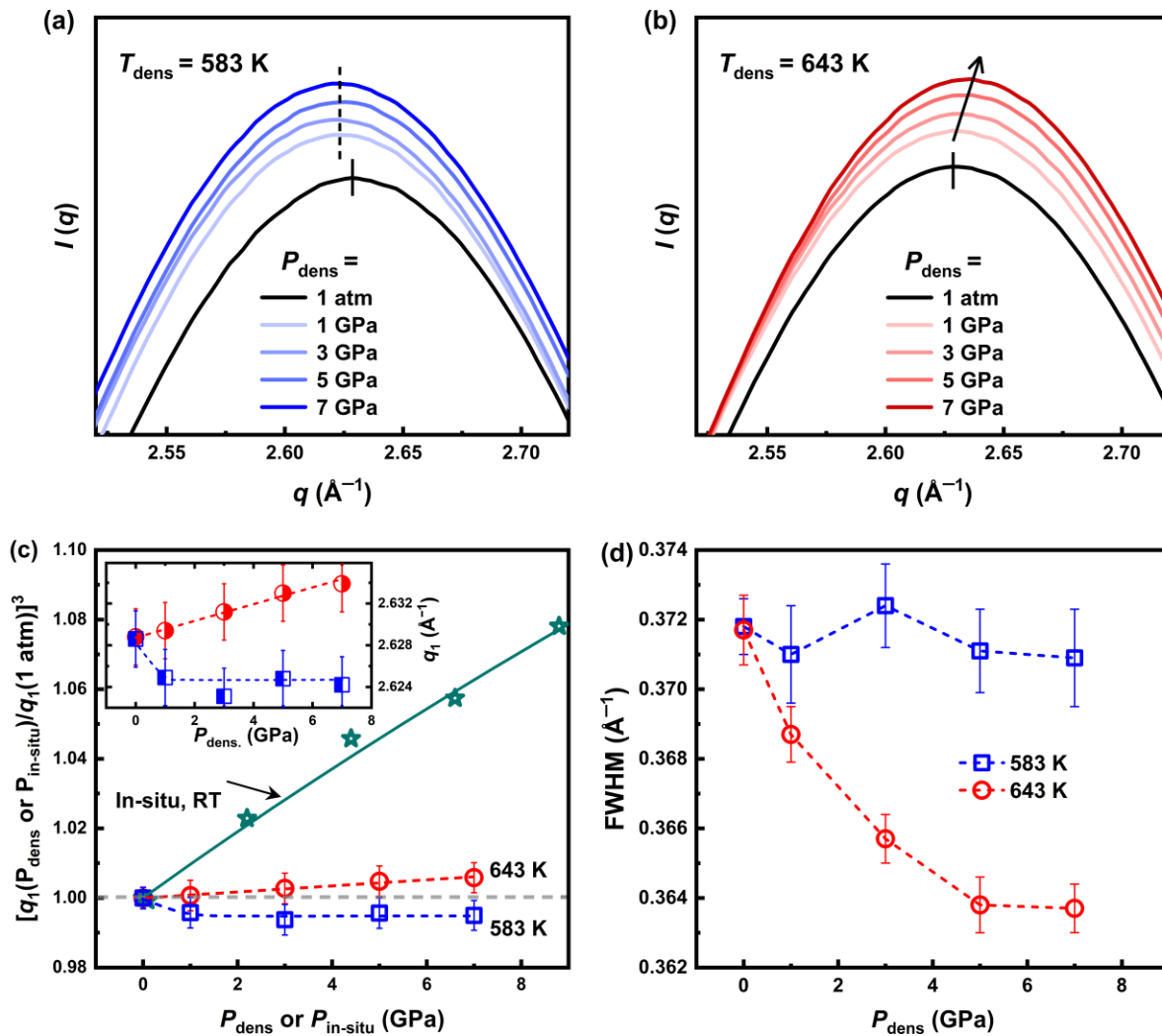


**Figure 5. Pressure dependence of the FSDP.** Intensity profile of glass samples compressed at different pressures and then measured at ambient temperature using synchrotron XRD. Measurements were performed



for  $T_{\text{dens}}$  **(a)** below  $T_g(1 \text{ atm})=596 \text{ K}$  and **(b)** above  $T_g(7 \text{ GPa})=634 \text{ K}$ . To differentiate the curves, a vertical offset was applied. Lines and arrow indicate the evolution of peak positions with increasing  $P_{\text{dens}}$ . **(c)** Pressure dependence of the FSDP  $q_1^3$  for a sample kept in-situ at different pressures values  $P_{\text{in-situ}}$ , and for the glasses of panel (a) and (b) previously compressed at different  $P_{\text{dens}}$  and  $T_{\text{dens}}$  and measured here at 1 atm. All data are rescaled by the reference value at 1 atm. The difference between the *in-situ* and *ex-situ* densifications provides an indication of the volume recovery after the decompression. The green line is the fit of a third-order equation of state for the *in-situ* data with a fitted bulk modulus of  $102 \pm 3 \text{ GPa}$ . The inset reports  $q_1$  value for different densified glasses of panel (a) and (b). **(d)** The evolution of the FWHM of the XRD data of panel (a) and (b).

To clarify this different densification process in the two dynamical ranges, we investigated the pressure dependence of glasses compressed at different values of  $P_{\text{dens}}$  in both the  $\beta$ -dominated regime at  $T_{\text{dens}} = 583 \text{ K}$  and in the liquid controlled by structural relaxation at  $643 \text{ K}$ . The intensity profiles of the maximum of the FSDP of the recovered glasses are shown in **Fig. 5a** and **5b** together with reference data pre-annealed at  $583 \text{ K}$  and  $643 \text{ K}$  at 1 atm (black lines). The center position of the FSDP,  $q_1$ , and the FWHM values were fitted using Gaussian functions within the same peak range (**Fig. S6**). In agreement with the previous data of **Fig. 3**, pressure significantly amplifies the relaxation response. Remarkably, we can clearly distinguish differences in the pre-compressed samples depending on whether the samples were compressed from the liquid or glassy state, or more specifically, whether sufficient degree of equilibration occurred before decompression. While constant peak position and FWHM are observed after densification in the glass, the maximum of the FSDP increases and the FWHM decreases with larger pressure values in the glasses compressed from the liquid phase. The effect is quantified in **Fig. 5c and 5d**, where we report the evolution of the cube of the center position of the FSDP,  $q_1^3$  and the FWHM. We remind that the inverse quantity  $1/q_1^3$  is often associated to density changes [54]. For a better comprehension, we report also data obtained with XRD during *in-situ* compression at high pressure with a diamond anvil cell (see Methods). These data provide information on the compressibility of the sample at room temperature.

The glasses recovered after compression in the liquid at  $T_{\text{dens}}=643$  K, exhibit an increase in  $q_1$  and a linear relationship with  $\left(\frac{\partial q_1}{\partial P_{\text{dens.}}}\right)_{T_{\text{dens.}}} \approx 0.0008 \text{ \AA}^{-1}/\text{GPa}$  within the applied  $P_{\text{dens.}}$  range, without showing signs of saturation in densification. This behavior reflects the increasing densification occurring in the sample kept at high pressure. However, when  $P_{\text{in-situ}}$  reaches 7 GPa, the  $q_1^3$  increases by approximately 6.3% compared to the pristine sample, while, the 7 GPa sample compressed in the liquid shows only about 0.6% permanent densification, indicating that most of the deformation is elastic and is recovered during the pressure release process.

In contrast, when compressed at 583 K, the resulting samples exhibit a lower  $q_1$  value, even lower than that of the 1 atm reference sample, in agreement with the structural expansion shown in **Fig. 3** and literature studies [34,35]. This is consistently observed for different  $P_{\text{dens.}}$ , with  $q_1$  remaining constant at an average value of  $2.624 \pm 0.001 \text{ \AA}^{-1}$ , representing a decrease of 0.17% compared to the 1 atm reference sample. Thus, unlike densification, the resulting material exhibits a novel configuration with a looser atomic packing structure at the level of the FSDP compared to the pristine state, independently of the applied pressure. A similar trend is confirmed also by the FWHM shown in **Fig. 5d**. At  $T_{\text{dens}}=643$  K, FWHM decreases as pressure increases, aligning with the trend observed for  $q_1$ , which indicates that densification and structural ordering occur simultaneously. In contrast, at  $T_{\text{dens}}=583$  K, the FWHM remains unchanged within the fitting error range, suggesting that in the glassy state, the compressed structure is independent of the applied pressure.

### **Discussion:**

Our densification experiments allow us to disentangle pressure and temperature effects on the structure and stability of compressed glasses, here indicated by the evolution of the  $T_f$  and the FSDP. Hydrostatic compression at room temperature has a weak influence on thermal properties, resulting in a small rejuvenation process, which instead can be significantly enhanced on increasing  $T_{\text{dens}}$  in the  $\beta$ -relaxation dominated regime, and which can be retained after decompression (**Fig. 2a** and **3e**). At the same time, the structure of the recovered glasses is more

expanded and disordered, at least over length scales of about  $\sim 10\text{\AA}$  and is independent on the applied pressure  $P_{dens}$  (**Fig. 3b, 3c** and **5c**). The XRD data show only a weak signature of an ordering process with increasing  $T_{dens}$  as signaled by the increased intensity in the first three coordination shells (**Fig. 4**). This implies that pressure modifies the short- and medium-range order of the glass and brings it towards a free energy minimum which must differ from that of the pristine material.

Furthermore, as shown also by recent simulations [15] and XPCS experiments [58] some liquid-like collective atomic dynamics are activated below  $T_g$  (around  $0.9 T_g$ ), corresponding to our observation that the rejuvenation effect begins to weaken when the  $\beta$ - to  $\alpha$ -relaxation transition occurs (**Fig. 3**). In this region, both fictive temperature and structural parameters are strongly influenced by  $T_{dens}$  reflecting the rapid variation in the activation energy of the involved relaxation process. However, while the structure exhibits a monotonic evolution toward a more compacted and homogenous configuration (**Fig. 3b** and **3c**),  $T_f$  abruptly drops, due to an acceleration of the aging induced by the  $\alpha$ -relaxation process (**Fig. 3e**). When  $T_{dens}$  exceeds  $T_g(P)$ , the complete activation of the  $\alpha$ -relaxation process ensures sufficient relaxation of the sample before decompression, resulting in a denser glass with enhanced stability, as signaled by the lower value of  $T_f$  with respect to the reference data at 1 atm. In this region,  $T_f$  is also independent on  $T_{dens}$  as all glasses are densified from the same equilibrium liquid phase. The non-monotonous evolution of  $T_f$  is a consequence of the different response to pressure of the  $\alpha$ - and  $\beta$ - relaxation and means that the degree of equilibration reached by the system is not a sufficient parameter to describe the stability of a glass (**Fig. 2a** and **Fig. S5**).

At the same time, the samples densified from the liquid phase exhibit a reduction in the radial distances of each atomic coordination shell, which is promoted for larger  $P_{dens}$ , typically leading to glass densification (**Fig. 5c**).

Consistent with previous findings in different MGs [34-36,59], hydrostatic compression in the Vit4 glassy state leads to a shift of the FSDP to larger length scales (see **Fig. 3a, 3d**). This phenomenon likely reflects a universal characteristic of MGs: pressure compels atoms into regions

with insufficient space, thereby expanding the nearest-neighbor atomic cages. Pan et al. demonstrated that the hydrostatic component of axial compression stress in notched specimens plays a critical role in achieving significant thermodynamic rejuvenation ( $T_f$  increases) and volume expansion at room temperature [35]. Based on our results, where samples are treated under pure hydrostatic pressure, the structural expansion appears to be more pronounced ( $q_1$  decreased by  $\sim 0.17\%$ ).

Although  $\beta$ -relaxation in Zr-based MGs (including Vit4) is characterized by an excess wing in the dynamic mechanical spectrum [8], which makes it difficult to distinguish it from  $\alpha$ -relaxation, in calorimetry it is assumed to be responsible for the observed sub- $T_g$  endothermic peak [45,52,53], and, for long annealing experiments well below  $T_g$  results in multiple steps of equilibrium recovery in various kinds of glasses [60,61], with the fast step mediated by the  $\beta$ -relaxation. Recent experiments have shown that the intensity of the sub- $T_g$  endothermic peak associated with  $\beta$ -relaxation can be amplified under fast heating conditions [52,53]. As shown in this study, fast calorimetry provides an opportunity to characterize the  $\beta$ -relaxation under high-pressure and to calculate its activation energy across a wide range of heating rates.

In summary, through densification experiments over a wide temperature range combined with subsequent calorimetric and X-ray diffraction analysis in real and reciprocal space, we studied the pressure and temperature response of the  $\alpha$ - and  $\beta$ -relaxations in a strong MG (Vit4) and its effect on the stability and structure of the recovered glasses.

We found that the degree of ergodicity reached by Vit4 during the compression significantly impacts the pressure response, leading to relaxation or rejuvenation depending if the relaxation process controlling the dynamics is the collective  $\alpha$ -relaxation process or the localized  $\beta$ -relaxation, respectively. When the dynamics are governed by the collective  $\alpha$ -relaxation process, the glass tends to undergo relaxation; in contrast, when dominated by the localized  $\beta$ -relaxation, the glass exhibits rejuvenation. This result rationalizes also our recent similar findings in a Pt-based MGs [34]. The pressure-sensitivity of the relaxation spectrum of Vit4 is reflected by the shift of the  $\beta$ - to  $\alpha$ -relaxation transition to higher temperatures with increasing pressure, which occurs always at

a specific degree of equilibration, as demonstrated by the scaling of the activation energies of the different processes onto a master curve based on  $T/T_g(P)$ . This relationship does not hold for the  $T_f$  due to the different pressure response of the two relaxation processes and due to the fact that the shift  $dT_g(P)/dP$  reflects only the pressure dependence of the  $\alpha$ -relaxation process. This implies that the degree of equilibration reached by the system is not a sufficient metric to define the stability of a glass and rescale all the dynamics as indeed is the case also for molecular and polymeric systems [46,50,60].

Combined with subsequent X-ray diffraction analysis, it further shows that  $\beta$ -relaxation promotes rejuvenation and is associated with a looser atomic packing independent of the applied pressure which appears to be independent on density, while the  $\alpha$ -relaxation process leads to glass stabilization through a pressure-dependent densification process, involving larger-scale structural rearrangements despite the very small permanent densification retrieved after the compression. Our results elucidate the role of pressure and temperature on the structure and stability in a prototypical strong metallic glass, allowing to formulate well-defined thermo-mechanical protocols to design glasses of the same composition and different properties. This is another important implication of our work that can be important in the development of new amorphous metals or in their application under external stimuli.

## **Methods**

Sample preparation and compression protocols: Element metals with a minimum purity of 99.99% were melted under a high-purity argon atmosphere to form the master alloy, following an atomic ratio of  $Zr_{46.25}Ti_{18.25}Cu_{7.5}Ni_{10}Be_{27.5}$ . Ribbons of the corresponding MGs with a thickness of  $30 \pm 2 \mu m$  were then produced by melt spinning the master alloy molten liquid under Ar atmosphere. The compression protocols were performed with a Belt press at the institute Néel, Grenoble, France. For this purpose, the ribbons were cut into  $2 \times 2 \text{ mm}^2$  H×V pieces and each compression was performed by inserting 10-20 pieces in a boron nitride (BN) capsule in different groups separated by small disks of BN. The capsules were then inserted in a graphite furnace and mounted in the

press, ensuring hydrostatic compression. Different densification protocols were performed in order to study separately the dependence of the material properties on the densification pressure  $P_{\text{dens}}$  in the (1-7) GPa pressure range at a fixed densification temperature,  $T_{\text{dens}}$ , and then the dependence of  $T_{\text{dens}}$  in the 298-693 K range while keeping  $P_{\text{dens}}$  fixed. For each sample, we first increased the pressure to  $P_{\text{dens}}$  and subsequently increased the temperature to  $T_{\text{dens}}$  for a 10-minute isotherm. The samples were then cooled to 298 K under pressure, and the pressure was released only after reaching ambient temperature. The heating/cooling rate and the compression/decompression rates were set to 20 K/min and 0.3 GPa/min, respectively.

Synchrotron XRD on compressed samples: The structure of the glasses recovered after the compression was measured at ID13 and ID15a beamlines at ESRF, Grenoble, France. At ID13, the X-ray beam energy was set at 13 keV and the diffraction data were collected using the Eiger X 4M detector using a beam size of  $2.5 \times 2.5 \text{ H} \times \text{V } \mu\text{m}^2$ . The detector-to-sample distance was set to 81.6 mm to achieve a detectable  $q$ -range of  $0.1\text{-}7 \text{ \AA}^{-1}$ , and ensuring sufficient resolution for the first diffraction peak with one point per  $0.003 \text{ \AA}^{-1}$ . A calibration was performed using a standard  $\alpha$ - $\text{Al}_2\text{O}_3$  material. Samples were mounted on a 3D-printed epoxy resin platform and kept at room temperature. To ensure robust statistical data, we collected approximately 1800 points of the sample with a  $5 \mu\text{m}$  interval between each point and an exposure time of 0.02 s per point. Subsequently, the diffraction intensities from all points were averaged, and the background noise generated by the air adjacent to the sample was subtracted. These data provided information on the structure in reciprocal space. In order to obtain the  $q_1$  and the FWHM for the FSDP of  $I(q)$ , we

employed Gaussian function fitting to the data:  $y = y_0 + \frac{A}{w \sqrt{\frac{\pi}{4 \times \log(2)}}} \times \exp(-4 \times \log(2) \times (\frac{x-x_c}{w})^2)$ , where  $y$

represents data from the first peak of  $I(q)$ ,  $x$  represents the  $q$  values,  $y_0$  is the baseline value,  $A$  is the amplitude of the function,  $x_c$  is  $q_1$ , and  $w$  is the FWHM of the peak. The discussion of the fitting results in relation to the fitting range of the data can be found in **Fig. S6** and **S7**.

Direct space analysis was instead performed by measuring the pair distribution functions,  $G(r)$ , at beamline ID15a using a 68.5 keV photon energy and a 145 mm detector-to-sample distance,

probing a 0.3-30  $\text{\AA}^{-1}$  detectable  $q$ -range.  $\text{CrO}_3$  was used for calibration prior to the measurements. The samples were fixed using copper clamps at ambient temperature. The scattered intensity was recorded with a Pilatus3 X CdTe 2M detector and each sample was exposed for 1 min to obtain good statistics. Diffraction patterns were azimuthally integrated using routines from the pyFAI library, and locally implemented corrections for the outlier rejection, background, polarization of the X-rays and detector geometry, response, and transmission, to yield 1D diffraction patterns. The structure factor,  $S(q)$ , was extracted from the scattered intensity  $I^C(q)$  as  $S(q)=1+\frac{I^C(q)-\langle f(q) \rangle^2}{\langle f(q) \rangle^2}$ , where  $\langle f(q) \rangle = \sum_{\alpha} c_{\alpha} f_{\alpha}(q)$  with  $f_{\alpha}(q)$  and  $c_{\alpha}$  the atomic form factor and atomic concentration for chemical species  $\alpha$ , respectively.  $G(r)$  were then obtained through a Fourier transform of the structure factor using the equation  $G(r)=\frac{2}{\pi} \int_0^{+\infty} q(S(q)-1)\sin(qr) dq$  by means of the PDFgetX2 software [62].

Synchrotron high-pressure XRD. Additional *in-situ* high-pressure measurements were conducted at P10 beamline at PETRA III in Hamburg, Germany. A pre-cut sample with the dimension of  $40 \times 40 \times 30 \text{ H} \times \text{V} \times \text{L} \mu\text{m}^3$  was loaded in a membrane diamond anvil cell (DAC) with helium as a pressure-transmitting medium, and the pressure was monitored from the fluorescence spectrum of a ruby sphere placed next to the sample. The X-ray energy was set to 15.0 keV and data were recorded using an EigerX 4M detector situated 1840 mm downstream from the sample. The pressurization/decompression rate was controlled by an automatic pressure driver with a rate of 0.2 bar/s. After reaching each isobaric stage, the pressure was maintained for at least 30 minutes with a stability better than 0.1 GPa and XRD data were continuously collected during this stage, with an exposure time of 0.5 s/frame.

Calorimetry: Thermal properties were studied using a FDSC (flash differential scanning calorimetry, Mettler Toledo, FDSC2+) apparatus with a heating rate of 100-1000 K/s. Measurements were conducted under a high-purity  $\text{N}_2$  flow of 80 ml/min. The measured samples were cut into pieces of  $\sim 80 \times 80 \times 30 \mu\text{m}^3$  and then transferred to the UFS chip of the calorimeter. Unlike the traditional melting-quenching-heating measurements, we used a single-shot method for

thermal analysis, with each sample being used only once. For each sample, at least two different sections were cut and measured independently to ensure reproducibility (**Fig. S1**).

In order to determine the mass of the sample in FDSC, we first conduct a DSC (Mettler Toledo, DSC3) measurement by using approximately 10 mg of the sample to assess the heat flow step,  $\Delta Q$ , which adheres to the formula  $\Delta Q = C_p * \Phi * m$ , where  $C_p$  represents the specific heat of the sample,  $\Phi$  is the heating rate, and  $m$  is the sample mass. By ascertaining the  $\Delta Q$  in FDSC, we can further verify the mass of the sample with the FDSC setup based on the sample  $C_p$ .

Fictive temperatures,  $T_f$ , were calculated using Moynihan's area-matching method [49] with the following equation:

$$\int_{T_f}^{T_1 \gg T_g} (C_{p, \text{liquid}} - C_{p, \text{glass}}) dT = \int_{T_2 \ll T_g}^{T_1 \gg T_g} (C_p - C_{p, \text{glass}}) dT \quad (1)$$

where  $C_{p, \text{liquid}}$  and  $C_{p, \text{glass}}$  represent the specific heat capacities of the liquid and glass, respectively. The endothermic peaks with different characteristic temperatures,  $T_p$  (**Fig. S2** shows the definition of  $T_p$ ), of the FDSC curve indicate relaxation processes. The Kissinger equation [63] of the different  $T_p$  and the  $\Phi$  were used to estimate the activation energies,  $E_a$ , of these processes:

$$\ln \left( \frac{\Phi}{T_p^2} \right) = - \frac{E_a}{RT_p} + a \quad (2)$$

where  $R$  is the gas constant and  $a$  is a constant.

## Acknowledgements

We gratefully acknowledge the ESRF (Grenoble, France) for providing beamtime, including experiments conducted during in-house beamtime (ihsc1815) at ID13 and the beamtime under the proposal HC4986 at ID15A. We also thank DESY (Hamburg, Germany), a member of the Helmholtz Association HGF, for providing the beamtime under the proposal 11016133EC beamline P10 at PETRA III. This project received funding from the European Research Council (ERC) under the European Union's Horizon 2020 research and innovation program (Grant Agreement No. 948780).



## Competing Interests

The authors declare that there are no financial or non-financial competing interests.

## Author Contributions

JS, AC, CG, and ML conducted the densification experiments. FY and EP provided the samples. JS, AC, AR, BR, GV, and MdM performed the PDF experiment, and GV and JS analyzed the data. JS and JL carried out the XRD experiment and analyzed the data. JS conducted the FDSC experiments and analyzed the results with the assistance of DC, JG, and GM. JS, AC, AR, and BR conducted the *in-situ* high-pressure XRD experiments with support from GG and FW. JS and BR wrote the manuscript with contributions from all authors. JS and AC contributed equally to this work. BR conceived the study and led the investigation.

## Reference

- [1] E. Donth, *The Glass Transition* (Springer, Berlin, 2001).
- [2] P. G. Debenedetti and F. H. Stillinger, Supercooled liquids and the glass transition, *Nature* (London) **410**, 259 (2001).
- [3] W. Kob and H. C. Andersen, Testing mode-coupling theory for a supercooled binary Lennard-Jones mixture. II. Intermediate scattering function and dynamic susceptibility, *Phys. Rev. E* **52**, 4134 (1995).
- [4] W. H. Wang, Dynamic relaxations and relaxation-property relationships in metallic glasses, *Prog. Mater. Sci.*, **106**, 100561 (2019).
- [5] Z. Y. Zhou, Q. Yang and H. B. Yu, Toward atomic-scale understanding of structure-dynamics-properties relations for metallic glasses, *Prog. Mater. Sci.* **145**, 101311 (2024).
- [6] C. A. Angell, Relaxation in liquids, polymers and plastic crystals—strong/fragile patterns and problems, *Journal of Non-Crystalline Solids*, **131**, 13–31 (1991).
- [7] H. B. Yu, R. Richert and K. Samwer, Structural rearrangements governing Johari-Goldstein

relaxations in metallic glasses, *Sci. Adv.* **3**, e1701577 (2017).

[8] H. B. Yu, W. H. Wang, H. Y. Bai and K. Samwer, The  $\beta$ -relaxation in metallic glasses, *Nat. Sci. Rev.* **1**, 429 (2014).

[9] Q. Yang et al., Structural length-scale of  $\beta$  relaxation in metallic glass, *J. Chem. Phys.* **157**, 184504 (2022).

[10] H. B. Yu, W. H. Wang, H. Y. Bai, Y. Wu and M. W. Chen, Relating activation of shear transformation zones to  $\beta$  relaxations in metallic glasses, *Phys. Rev. B*, **81**, 220201 (2010).

[11] Q. Wang et al., Unusual fast secondary relaxation in metallic glass, *Nature Commun.* **6**, 7876 (2015).

[12] S. Küchemann and R. Maaß, Gamma relaxation in bulk metallic glasses. *Scr. Mater.*, **137**, 5–8 (2017).

[13] B. Wang et al., Understanding atomic-scale features of low-temperature relaxation dynamics in metallic glasses, *J. Phys. Chem. Lett.* **7**, 4945–4950 (2016).

[14] C. Chang et al., Liquid-like atoms in dense-packed solid glasses, **21**, 1240–1245 (2022).

[15] D. Şopu, X. Yuan, F. Spieckermann and J. Eckert, Coupling structural, chemical composition and stress fluctuations with relaxation dynamics in metallic glasses, *Acta Mater.* **275**, 15 (2024).

[16] Z. Evenson et al.,  $\beta$  relaxation and low-temperature aging in a Au-based bulk metallic glass: From elastic properties to atomic-scale structure, *Phys. Rev. B* **89**, 174204 (2014).

[17] L. J. Song et al., Activation entropy as a key factor controlling the memory effect in glasses, *Phys. Rev. Lett.* **125**, 135501 (2020).

[18] S. Y. Zhang et al., Decoupling between enthalpy and mechanical properties in rejuvenated metallic glass, *Scripta Mater.* **223**, 115056 (2023).

[19] Spieckermann F et al., Structure-dynamics relationships in cryogenically deformed bulk metallic glass, *Nature Commun.* **13**, 127 (2022).

[20] V.M. Giordano and B. Ruta, Unveiling the structural arrangements responsible for the atomic dynamics in metallic glasses during physical aging, *Nature Commun.* **7**, 10344 (2016).

[21] M. Paluch, B. B. Yao, J. Pionteck and Z. Wojnarowska, Predicting the density-scaling

exponent of a glass-forming liquid from complex dielectric permittivity measurements, *Phys. Rev. Lett.* **131**, 086101 (2023).

[22] R. Casalini and C. M. Roland, Temperature and density effects on the local segmental and global chain dynamics of poly(oxybutylene), *Macromolecules*, **38**, 1779–1788 (2005).

[23] Z. Wojnarowska et al., Pressure-induced liquid-liquid transition in a family of ionic materials, *Nature Commun.* **13**, 1342 (2022).

[24] R. Casalini and C. M. Roland, Communication: Effect of density on the physical aging of pressure-densified polymethylmethacrylate, *J. Chem. Phys.* **147**, 091104 (2017).

[25] M. Paluch et al., Does the Arrhenius temperature dependence of the Johari-Goldstein relaxation persist above  $T_g$ ? *Phys. Rev. Lett.* **91**, 115701 (2003).

[26] A. Cornet et al., High-pressure X-ray photon correlation spectroscopy at fourth-generation synchrotron sources, *J. Synchrotron Rad.* **31**, 527–539, (2024).

[27] Y. C. Hu et al., Pressure effects on structure and dynamics of metallic glass-forming liquid, *J. Chem. Phys.* **146**, 024507 (2017).

[28] T. Rouxel, H. Ji, T. Hammouda and A. Moréac, Poisson's ratio and the densification of glass under high pressure, *Phys. Rev. Lett.* **100**, 225501 (2008).

[29] T. P. Ge et al., Unusual energy state evolution in Ce-based metallic glass under high pressure, *J. Appl. Phys.* **121**, 205109 (2017).

[30] R. J. Xue et al., Enhanced kinetic stability of a bulk metallic glass by high pressure, *Appl. Phys. Lett.* **109**, 221904 (2016).

[31] S. Chen et al., Reversible linear-compression behavior of free volume in a metallic glass, *Phys. Rev. B* **105**, 144201 (2022).

[32] K. Samwer, R. Busch and W. L. Johnson, Change of compressibility at the glass transition and Prigogine-Defay ratio in ZrTiCuNiBe alloys, *Phys. Rev. Lett.* **82**, 580–583 (1999).

[33] H. J. Jin, X. J. Gu, P. Wen, L. B. Wang and K. Lu, Pressure effect on the structural relaxation and glass transition in metallic glasses, *Acta Mater.* **51**, 6219–6231 (2003).

[34] A. Cornet et al., Break-down of the relationship between  $\alpha$ -relaxation and equilibration in

hydrostatically compressed metallic glasses, arXiv:2409.13636v1 (2024).

[35] J. Pan, Y. P. Ivanov, W. H. Zhou, Y. Li and A. L. Greer, Strain-hardening and suppression of shear-banding in rejuvenated bulk metallic glass, *Nature* **578**, 559–562 (2020).

[36] W. Dmowski et al., High Pressure Quenched Glasses: unique structures and properties, *Sci. Rep.* **10**, 9497 (2020).

[37] C. Wang et al., High stored energy of metallic glasses induced by high pressure, *Appl. Phys. Lett.* **110**, 111901 (2017).

[38] A. Cornet et al., Denser glasses relax faster: Enhanced atomic mobility and anomalous particle displacement under in-situ high pressure compression of metallic glasses, *Acta Mater.*, **255**, 119065 (2023).

[39] H. B. Zhou et al., X-ray photon correlation spectroscopy revealing the change of relaxation dynamics of a severely deformed Pd-based bulk metallic glass, *Acta Mater.* **195**, 446–453 (2020).

[40] B. Ruta et al., Atomic-scale relaxation dynamics and aging in a metallic glass probed by X-ray photon correlation spectroscopy, *Phys. Rev. Lett.* **109**, 165701 (2012).

[41] Y. T. Sun et al., Distinct relaxation mechanism at room temperature in metallic glass, **14**, 540 (2023).

[42] Z. Wang, B. A. Sun, H. Y. Bai and W. H. Wang, Evolution of hidden localized flow during glass-to-liquid transition in metallic glass, *Nature Commun.* **5**, 5823 (2014).

[43] X. Monnier, D. Cangialosi, B. Ruta, R. Busch, and I. Gallino, Vitrification decoupling from  $\alpha$ -relaxation in a metallic glass. *Sci. Adv.* **6**, eaay1454 (2020).

[44] N. Amini et al., Intrinsic relaxation in a supercooled ZrTiNiCuBe glass forming liquid, *Phys. Rev. Mater.* **5**, 055601 (2021).

[45] L. J. Song, W. Xu, J. T. Huo, J. Q. Wang, X. M. Wang and R. W. Li, Two-step relaxations in metallic glasses during isothermal annealing, *Intermetallics*, **93**, 101–105 (2018).

[46] D. Cangialosi, Physical aging and vitrification in polymers and other glasses: Complex behavior and size effects. *Journal of Polymer Science* **62**, 1952–1974 (2024).

[47] Y. Z. Yue and C. A. Angell, Clarifying the glass-transition behaviour of water by comparison

with hyperquenched inorganic glasses, *Nature* **427**, 717–720 (2004).

[48] N. G. Perez-De Eulate and D. Cangialosi, The very long-term physical aging of glassy polymers, *Phys. Chem. Chem. Phys.* **20**, 12356–12361 (2018).

[49] C. T. Moynihan, A. J. Easteal, M. A. De Bolt and J. Tucker, Dependence of the fictive temperature of glass on cooling rate, *J. Am. Ceram. Soc.* **59**, 12–16 (1976).

[50] V. Di Lisio, V. M. Stavropoulou, D. Cangialosi, Physical aging in molecular glasses beyond the  $\alpha$  relaxation, *J. Chem. Phys.*, 064505, 159, (2023).

[51] J. Jiang et al., Decoupling between calorimetric and dynamical glass transitions in high-entropy metallic glasses, *Nature Commun.* **12**, 3843 (2021).

[52] M. Gao and J. H. Perepezko, Separating  $\beta$  relaxation from  $\alpha$  relaxation in fragile metallic glasses based on ultrafast flash differential scanning calorimetry, *Phys. Rev. Mater.* **4**, 025602 (2020).

[53] Q. Yang, S. X. Peng, Z. Wang and H. B. Yu, Shadow glass transition as a thermodynamic signature of  $\beta$  relaxation in hyper-quenched metallic glasses, *Natl. Sci. Rev.* **7**, 1896–1905 (2020).

[54] A. R. Yavari et al., Excess free volume in metallic glasses measured by X-ray diffraction, *Acta Mater.* **53**, 1611 (2005).

[55] A. K. Sinha and P. Duwez, Radial distribution function of amorphous Ni-Pt-P alloys, *J. Phys. Chem. Solids* **32**, 267–277 (1971).

[56] Y. H. Meng et al., Rejuvenation by enthalpy relaxation in metallic glasses, *Acta Mater.* **241**, 118376 (2022).

[57] S. Sato et al., Effect of Al on local structures of Zr–Ni and Zr–Cu metallic glasses, *Mater. Trans.* **46**, 2893–2897 (2005).

[58] M. Frey et al. On the interplay of liquid-like and stress-driven dynamics in a metallic glass former observed by temperature scanning XPCS, arXiv preprint arXiv:2403.12306 (2024).

[59] H. F. Poulsen, J. A. Wert, J. Neufeind, V. Honkimäki and M. Daymond, Measuring strain distributions in amorphous materials, *Nature Mater.* **4**, 33–36. (2005).

[60] D. Cangialosi, V. M. Boucher, A. Alegría and J. Colmenero, Direct evidence of two

equilibration mechanisms in glassy polymers. *Phys. Rev. Lett.* **111**, 095701 (2013).

[61] R. Golovchak, A. Kozdras, V. Balitska and O. Shpotyuk, Step-wise kinetics of natural physical ageing in arsenic selenide glasses. *Journal of Physics: Condensed Matter* **24**, 505106 (2012).

[62] X. Qiu, J. W. Thompson and S. J. L. Billinge, PDFgetX2: a GUI-driven program to obtain the pair distribution function from X-ray powder diffraction data, *J. Appl. Cryst.* **37**, 678 (2004).

[63] H. S. Chen, On mechanisms of structural relaxation in a  $\text{Pa}_{48}\text{Ni}_{132}\text{P}_{20}$  glass, *J. Non-Crystal. Solids* **46**, 289 (1981).